SiO v = 1 J = 5 → 4 Maser Emission from the Root of the "Water Fountain" Source W 43A

The Astrophysical Journal, 987:114 (7pp), 2025 July 10 https://doi.org/10.3847/1538-4357/adde4e

SiO $v = 1 J = 5 \rightarrow 4$ Maser Emission from the Root of the "Water Fountain" Source W 43A

Hiroshi Imai[1,2], Takeshi Hoshino[3], Daniel Tafoya[4], José F. Gómez[5], Jun-ichi Nakashima[6,7], and Gabor Orosz[8]
[1] Amanogawa Galaxy Astronomy Research Center, Graduate School of Science and Engineering, Kagoshima University, 1-12-35 Korimoto, Kagoshima 890-0065, Japan; hiroimai@km.kagoshima-u.ac.jp
[2] Center for General Education, Institute for Comprehensive Education, Kagoshima University, 1-12-30 Korimoto, Kagoshima 890-0065, Japan
[3] Faculty of Science, Kagoshima University, 1-12-35 Korimoto, Kagoshima 890-0065, Japan
[4] Department of Space, Earth and Environment, Chalmers University of Technology, Onsala Space Observatory, 439 92 Onsala, Sweden
[5] Instituto de Astrofísica de Andalucía, CSIC, Glorieta de la Astronomía s/n, E-18008 Granada, Spain
[6] School of Physics and Astronomy, Sun Yat-sen University, Tang Jia Wan, Zhuhai 519082, People's Republic of China
[7] CSST Science Center for the Guangdong-Hong Kong-Macau Greater Bay Area, 67 Sun Yat-Sen University, 2 Duxue Road, Zhuhai 519082, Guangdong Province, People's Republic of China
[8] Joint Institute for VLBI ERIC, Oude Hoogeveensedijk 4, 7991 PD Dwingeloo, The Netherlands
Received 2025 February 21; revised 2025 May 11; accepted 2025 May 27; published 2025 July 2

Abstract

We report here the first mapping of SiO $v = 1$ $J = 5 \rightarrow 4$ maser emission toward the "water fountain" source W 43A in order to explore the central stellar system driving the collimated, bipolar, fast jet. The maser source has a systemic line-of-sight velocity consistent with that of CO $J = 2 \rightarrow 1$ emission tracing the jet within $\sim$2 km s^{-1} but a velocity gradient opposite that of the jet. The dynamical center of the maser source is located within $\sim$10 mas (or $\sim$20 au) of the brightness peak of the central 1.3 mm continuum emission. The spatiokinematic properties of the SiO $J = 5 \rightarrow 4$ and $J = 1 \rightarrow 0$ masers suggest that they are associated with the root of a slow (10 km s^{-1} $< V_{\rm outflow} <<$ 100 km s^{-1}) outflow with a large opening angle, and the central stellar system is contained within the inner maser region ($\sim$20 au) during a possible common-envelope evolution.

Unified Astronomy Thesaurus concepts: Circumstellar masers (240); Stellar jets (1607); Stellar mass loss (1613); Common envelope evolution (2154)

1. Introduction

SiO masers are expected to probe the innermost region of envelopes associated with the final evolution of stars such as asymptotic giant branch (AGB) and post-AGB stars. However, in rare cases, they are hosted by massive young stellar objects, in which they exhibit clearly bipolar spatiokinematics (see the review of M. Gray 2012). An interesting question is how such bipolar SiO masers can trace the evolution of the bipolar stellar outflows in their possibly short duration ($\lesssim$1000 yr).

SiO masers are also hosted by highly collimated, fast ($\geqslant$100 km s^{-1}), bipolar jets from dying stars, which are traced by H_2O masers (in 22 GHz, e.g., J. F. Gómez et al. 2017; in 321 GHz, D. Tafoya et al. 2014) and called as "water fountains" (WFs). WFs have extremely short dynamical ages (a few 100 yr) but extremely high stellar mass-loss rates (up to 10^{-3} $M_\odot$ yr^{-1}), so they play an unignorable role in mass recycling from stars to interstellar space (T. Khouri et al. 2021). H. Imai et al. (2005) mapped for the first time SiO $v = 1$ $J = 1 \rightarrow 0$ masers toward one of the WFs, W 43A. This source comprises a collimated jet and a spherically expanding circumstellar envelope (CSE), which are traced by H_2O and 1612 MHz OH masers, respectively (H. Imai et al. 2002). On the other hand, the velocity structure of the SiO masers was modeled as a wide-angle ($\theta_{\rm full} \sim 40°$), biconical, moderate-speed ($V_{\rm exp}\sim$ 30 km s^{-1}) outflow, seeming to solve the discrepancy of the line-of-sight (LoS) velocity gradients between the H_2O and OH masers with a model of a wide-angle biconical nozzle of the jet (H. Imai et al. 2005). It also supports the idea that the jet is driven and collimated by a magnetohydrodynamical force (W. H. T. Vlemmings et al. 2006), and the biconical nozzle emission may be connected to the material entrained and accelerated by the jet (S.-N. Chong et al. 2015; D. Tafoya et al. 2020, hereafter Paper I).

It has been suggested that WFs are the result of common-envelope evolution (CEE) in binary or multiple systems whose primary component has a relatively low initial mass (<4 $M_\odot$; T. Khouri et al. 2021). Spatially resolving the stellar systems comprising WFs is observationally challenging, since they are far away from the Sun ($D \geqslant 2$ kpc). However, it is possible to explore such systems from the spatiokinematic properties of their jets. The hypothesis of the CEE system is supported by periodic patterns of H_2O maser and CO emission (e.g., G. Orosz et al. 2019; Paper I) and/or a rapid growth of the length of the H_2O maser distribution over short timescales of around a decade (e.g., S.-N. Chong et al. 2015; H. Imai et al. 2020). However, one needs more direct evidence for a possible binary of a host giant star providing the material and its companion generating the jet with the provided material. The millimeter CO emission from the CSE is optically thick, making it difficult to resolve and trace the central system using these molecular lines. Moreover, H_2O maser emission in WFs always traces material far away ($\gtrsim$100 au) from the stellar system.

In this paper, we present the SiO $v = 1$ $J = 5 \rightarrow 4$ and $J = 1 \rightarrow 0$ masers associated with W 43A and observed with the Atacama Large Millimeter-submillimeter Array (ALMA) and the Very Large Array (VLA), respectively. Although the SiO $v = 1$ $J = 1 \rightarrow 0$ masers in W 43A have recently vanished (H. Imai et al. 2023), we detected SiO $v = 1$ $J = 5 \rightarrow 4$ masers

for the first time in this source, which provide a new probe to explore the central stellar system. In particular, we discuss the origin of the maser spatiokinematics in order to understand the nature of the central stellar system driving both the collimated fast jet (whose material should be supplied from either a companion star or an envelope of a collapsing star) and the slow outflow.

2. ALMA and VLA Observations

2.1. The ALMA Observation

The present ALMA observation was conducted in the project code 2018.1.00190.S on 2019 July 13 toward W 43A, a phase-referencing source J1851+0035, and other standard calibrators for ~1.5 hr in total. The frequency range of Band-6 (217–234 GHz) was observed including 1.3 mm continuum emission (mainly at the center frequency of 230.9 GHz with a bandwidth of 470 MHz) and spectral lines such as SiO $v = 1$ $J = 5 \rightarrow 4$. Although this paper presents only the maser data, the Appendix gives a list of other detected molecular lines. The phase-tracking center toward W 43A for the present ALMA observation was set to (R.A., decl.) (J2000.0) = $18^{h}47^{m}41\overset{s}{.}1631$, $-01°45'11\overset{''}{.}472$).

The postcorrelation process of the data was conducted in the normal manner in the CASA pipeline processed in the Joint ALMA Observatory, preserving the information of the absolute coordinates of the detected sources with respect to the phase-referencing calibrator. In order to further improve the signal-to-noise ratios of the detected emission, we employed the self-calibration using the bright continuum emission of W 43A in spectral channels that are free from any line emission. The calibration solutions were applied to all the provided visibility data.

As a result, the final continuum image and the image cubes of spectral lines were obtained with a synthesized beam with major and minor axes of 59 and 40 mas, respectively, at a position angle of 51°, and rms noise levels of 40 μJy beam^{-1} and 1.4 mJy beam^{-1} for the continuum map and the image cubes, respectively. The image cube of the SiO $v = 1$ $J = 5 \rightarrow 4$ maser data has 90 selected, consecutive spectral channels each with a velocity spacing of 0.79 km s^{-1}. The image cubes of other spectral lines will be presented in separate papers.

2.2. The VLA Observation

The present VLA observation was conducted in the project code AI113 on 2004 December 7, ~1.5 yr after the observation published by H. Imai et al. (2005). Using 27 25 m telescopes, W 43A, a phase-referencing calibrator J1851+0035, and other standard calibrators were observed for ~5 hr in total. The 7 mm band around 43.11 GHz was observed in a total bandwidth of 25 MHz including 7 mm continuum emission, in which a subband of 6.25 MHz was divided into 32 spectral channels for the SiO $v = 1$ $J = 1 \rightarrow 0$ maser line. The phase-tracking center toward W 43A for the present VLA data was set to (R.A., decl.) (J2000.0) = $18^{h}47^{m}41\overset{s}{.}1618$, $-01°45'11\overset{''}{.}538$).

The postcorrelation process of the data was conducted using the Astronomical Image Processing System (AIPS) in the normal manner for the data calibration, including phase-referencing to the calibrator. The calibration solutions were applied to the data of W 43A for detecting faint emission toward it. Because the 7 mm continuum emission has been known to be spatially resolved out significantly in high angular resolution (H. Imai et al. 2005; see also B. H. K. Yung et al. 2017), this paper focuses its main attention on only the SiO masers. The masers were too faint to perform self-calibration. The final maser image cube was obtained with a synthesized beam with major and minor axes of 70 and 47 mas, respectively, at a position angle of 18°, and an rms noise level of ~3 mJy beam^{-1} in a velocity resolution of 1.36 km s^{-1}.

3. Results

3.1. Secular Proper Motion and Distance to W 43A Derived from the Continuum Source

Figure 1 shows the 1.3 mm continuum emission source toward W 43A. The whole brightness distribution has changed since the previous observation (Paper I), indicating the evolution of the collimated jet covered by the continuum emission region seen in this figure. The jet evolution found will be described in more detail in a separate paper (T. Hoshino et al. 2025, in preparation).

In this paper, we focus our main attention on the central peaked component of the continuum source that should host the stellar system in W 43A. Using this continuum component, we can determine the secular proper motion of and estimate the kinematic distance to W 43A more reliably. With the present data, we determined the position of the continuum peak on 2019 July 13 to be (R.A., decl.) (J2000.0) = $18^{h}47^{m}41\overset{s}{.}16257 \pm 0\overset{s}{.}00002$, $-01°45'11\overset{''}{.}5525 \pm 0\overset{''}{.}0003$). We also revisited the data already published by Paper I and determined the position of the same peak on 2017 September 22 to be (R.A., decl.) (J2000.0) = $18^{h}47^{m}41\overset{s}{.}16379 \pm 0\overset{s}{.}00004$, $-01°45'11\overset{''}{.}5427 \pm 0\overset{''}{.}0005$. Thus, a proper motion of the continuum source is derived to be ($\mu_{\rm R.A.}$, $\mu_{\rm decl.}$) = (-10.3 ± 0.4, -5.8 ± 0.3) [mas yr^{-1}]. Note that the possible modulation by the annual parallax is corrected for the derived proper motion. This suggests that W 43A should be located at a near distance in the solar circle of the the Milky Way but with some deviation from a circular Galactic rotation, as addressed later.

Here we employ the parallax-based distance calculator (M. J. Reid et al. 2016)[9] to estimate the distance to W 43A, which is basically based on the kinematic distance method using the derived proper motion mentioned above as well as the systemic LoS velocity (with respect to the local standard of rest, LSR) derived from the CO emission, $V_{\rm LSR} = 34$ km s^{-1} (Paper I), well consistent with that from the 1612 MHz OH masers (H. Imai et al. 2002), and an assumption of the Galactic rotation mentioned above. The derived distance is 2.0 ± 0.3 kpc, consistent with that previously derived (Paper I). Here note that the derived proper motion does not contribute actually so much to improving the distance accuracy. We note that W 43A is not a young stellar object, even though it is close to the Galactic midplane ($|b| \simeq 0\overset{\circ}{.}0$) and to the star-forming region W 43. In fact, in the same manner as that by H. Imai et al. (2007), we obtained a large deviation of its motion from the Galactic flat rotation: (V_R, V_θ, V_z) = (47 ± 9, 48 ± 11, 69 ± 10) [km s^{-1}]. Even though young stellar objects may have some deviations in their secular motions from the Galactic rotation, these values are

[9] http://bessel.vlbi-astrometry.org/node/378

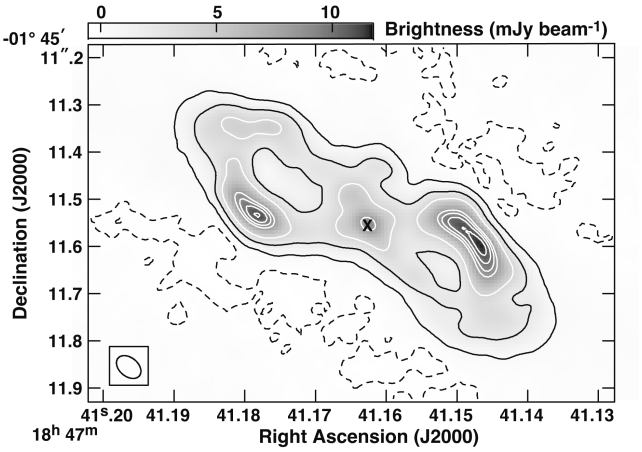

Figure 1. Brightness distribution of 1.3 mm continuum emission toward W 43A. The contour levels are −0.2, 0.5, 2, 4, 8, 9, 10, and 11 mJy beam^{-1}. The central cross denotes the peak of the continuum brightness at (R.A., Decl.) (J2000.0) = $18^{h}47^{m}41^{s}.1626$, $-01°45'11''.553$).

Table 1
Parameters of the Detected SiO $v = 1$ $J = 5 \rightarrow 4$ Maser Spots in W 43A

V_{LSR} (km s^{-1})	X (mas)	σ_X	Y (mas)	σ_Y	I_{Peak} (mJy beam^{-1})	$\sigma_{I_{Peak}}$
42.1	−34.24	5.57	−88.62	3.74	7.10	1.41
41.4	−34.61	4.04	−88.35	2.61	8.86	1.40
39.4	−47.09	10.51	−94.06	6.05	7.82	1.35
38.7	−42.94	5.10	−94.18	3.93	8.21	1.38
38.0	−26.07	4.78	−83.78	3.54	8.56	1.38
33.9	17.16	5.37	−77.81	2.85	7.95	1.42
30.6	17.85	5.60	−69.78	3.02	8.62	1.40
29.2	24.67	4.18	−72.59	2.86	9.34	1.42

Note. All the maser spots were detected over a 5σ noise level. The first column gives the LSR velocity of the maser spot. The second and the third columns give the R.A. offset and its error of the maser spot with respect to the delay-tracking center of the ALMA data correlation (see the main text). The fourth and the fifth columns give the decl. offset and its error of the maser spot. The sixth and the seventh columns give the peak intensity and its error of the maser spot.

still small, especially in the direction perpendicular to the Galactic plane ($V_z \lesssim 30$ km s^{-1}, N. Sakai et al. 2022).

Finally note that the astrometric error mentioned above includes only a statistic error scaled by a signal-to-noise ratio of the detected emission and the synthesized beam size. According to ALMA proposer's guide,[10] including a possible systematic error, the astrometric error would be up to ∼5 mas. Thus the uncertainty in the derived parameters may be larger, although we could find the proper motion of the continuum peak and the derived kinematic distance is consistent with those previously derived.

3.2. SiO v = 1 J = 5 → 4 Masers in W 43A

While we marginally detected SiO $v = 1$ $J = 5 \rightarrow 4$ masers in W 43A in the previous ALMA data taken in 2017 (Paper I), this paper shows clearer detection of the masers and their spot (velocity channel component) distribution. Table 1 gives the parameters of the maser spots detected in 2019. Figure 2 shows the distribution of the maser spots.

It is clear that the LoS velocity gradient is opposite that of the CO $J = 2 \rightarrow 1$ emission along the collimated jet extending to ∼0.″8 from its dynamical center at a position angle of ≈68° (Paper I). The LoS velocity gradient is also opposite that of the $J = 1 \rightarrow 0$ masers, while the velocity coverage of the $J = 5 \rightarrow 4$ masers ($26 \leqslant V_{LSR} \leqslant 42$ km s^{-1}) is a little narrower than that of the $J = 1 \rightarrow 0$ masers ($15 \leqslant V_{LSR} \leqslant 55$ km s^{-1}; J.-I. Nakashima & S. Deguchi 2003) and the maser spot distribution of the $J = 5 \rightarrow 4$ masers is much larger than that of the $J = 1 \rightarrow 0$ masers (∼100 and ∼15 mas, respectively; H. Imai et al. 2005; see also Section 3.3). Note that the LoS velocity gradient and the velocity coverage and the angular extent of the distribution of $J = 5 \rightarrow 4$ maser spots are more or less are consistent with those of 1612 MHz OH masers, tracing a CSE expanding at a velocity of ∼10 km s^{-1} and with an angular radius of ∼0.″2 (H. Imai et al. 2002).

The dynamical center of the outflow hosting the $J = 5 \rightarrow 4$ masers, namely, a midpoint between, e.g., the most blue- and redshifted maser spots with respect to the systemic velocity (V_{LSR} = 34 km s^{-1}), is coincident with the brightness peak of the central continuum source within ∼10 mas or 20 au.

3.3. SiO v = 1 J = 1 → 0 Masers in W 43A

SiO $v = 1$ $J = 1 \rightarrow 0$ masers in W 43A were confirmed to be visible until 2004 December, as shown in this paper, but seem to have vanished since 2005, when High Sensitivity Array observations were conducted (H. Imai et al. 2025, in private communication; see also H. Imai et al. 2023). Table 2 gives the parameters of the detected maser spots in 2004 December. Figure 3 shows the distribution of the maser spots.

The LoS velocity distribution of the maser spots looks random, but one can still see roughly a velocity gradient along the jet's axis (PA ≈ 68°), consistent with that found in the previous observation (H. Imai et al. 2023). As already mentioned in Section 3.2, the red-/blueshifted lobes are more consistent with CO than the SiO $v = 1$ $J = 5 \rightarrow 4$ masers. Note that the width of the maser spot distribution (⩽15 mas) is comparable to that of the SiO $v = 1$ $J = 5 \rightarrow 4$ masers in the direction perpendicular to the jet's axis (Section 3.2).

We attempted to estimate the location of the 1.3 mm continuum source (Section 3.1) in the map of SiO $v = 1$ $J = 1 \rightarrow 0$ masers in this paper. Extrapolating the continuum source position using the proper motion mentioned above, the continuum location is derived to be (∼180, ∼20) [mas] in Figure 3. Also note that the dynamical center of the masers found by H. Imai et al. (2005) is located ∼80 mas north from that found in this paper, outside the frame of Figure 3. These large position discrepancies should be carefully discussed, but we speculate that it may come from either an unknown systematic error in the derived proper motion mentioned in Section 3.1 (a possible position error of up to ∼70 mas taking into account the time baseline of ∼14 yr) or a large error in the absolute astrometry in the VLA data for the source close to the celestial equator, or both. In this case, one cannot rule out the possibility that both the SiO $v = 1$ $J = 5 \rightarrow 4$ and $J = 1 \rightarrow 0$ maser sources are commonly associated with the driving source of the jet.

[10] See https://almascience.nao.ac.jp/proposing/proposers-guide#appA:astrometry, A9.5 for Cycle-11.

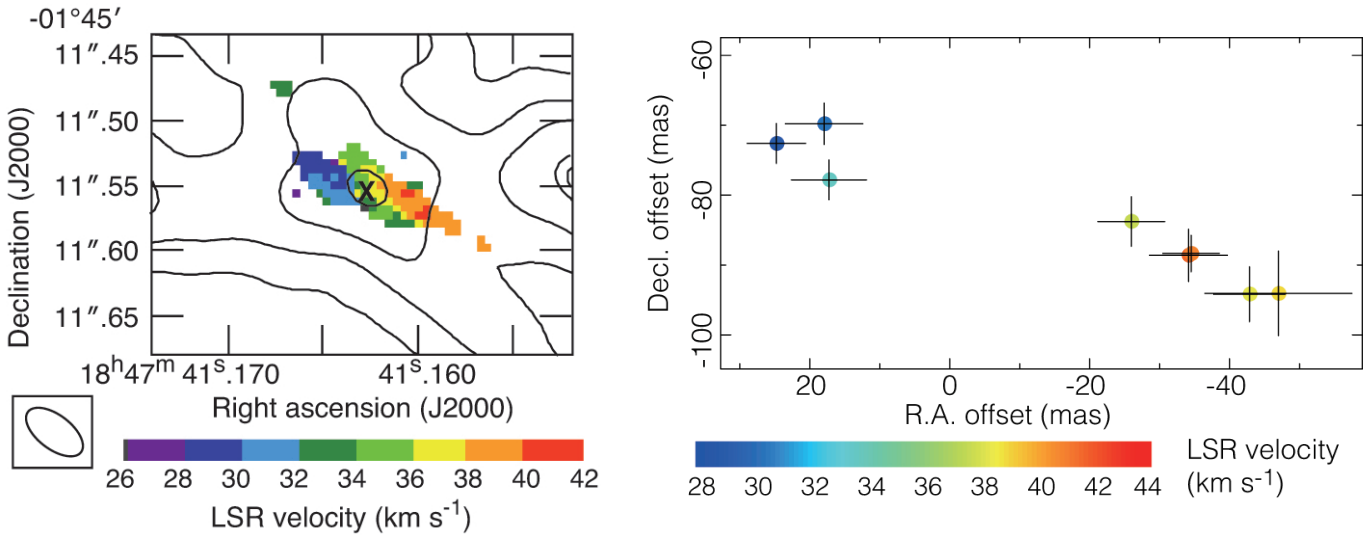

Figure 2. Distribution of SiO $v = 1$ $J = 5 \rightarrow 4$ maser emission in W 43A. Left: first moment map of the maser emission. The pixel size is 6 mas. Only the emission brighter than a 4σ noise level is integrated. The synthesized beam pattern and a color bar indicating the LSR velocity are shown below the diagram. The cross and background black contours are the same as those in Figure 1. Right: zoom-in view of the maser spot distribution with respect to the delay-tracking center of the ALMA data correlation (see the main text). The size of the plus bar indicates the position error of the spot.

Table 2
Parameters of the Detected SiO $v = 1$ $J = 1 \rightarrow 0$ Maser Spots in W 43A

$V_{\rm LSR}$ (km s^{-1})	X (mas)	σ_X	Y (mas)	σ_Y	$I_{\rm Peak}$ (Jy beam^{-1})	$\sigma_{I_{\rm Peak}}$
50.37	30.06	3.39	−3.18	4.82	0.02	0.003
47.65	24.77	2.08	−1.35	3.31	0.04	0.003
46.29	25.98	1.40	0.80	1.69	0.05	0.003
44.94	27.63	0.96	4.84	1.23	0.07	0.003
43.58	27.55	0.78	5.07	1.07	0.10	0.003
42.22	25.24	0.16	6.98	0.22	0.52	0.004
40.86	25.28	0.17	7.39	0.23	0.47	0.003
39.51	24.94	0.55	9.29	0.71	0.14	0.003
38.15	23.38	1.45	−2.94	1.97	0.05	0.003
35.43	26.20	3.32	12.36	4.37	0.02	0.003
31.36	17.96	1.46	2.46	2.15	0.05	0.003
30.00	18.09	0.98	−3.02	1.35	0.08	0.003
28.64	16.87	1.42	−1.92	2.03	0.05	0.003
27.28	18.72	0.65	−0.65	0.87	0.12	0.003
25.93	17.79	0.86	−0.92	1.11	0.10	0.003
24.57	18.93	0.40	0.18	0.56	0.17	0.003
23.21	16.89	0.88	−0.32	1.16	0.09	0.003
21.85	16.40	0.85	3.25	1.20	0.09	0.003
20.50	15.11	1.32	0.21	1.82	0.06	0.003
19.14	13.69	2.04	−4.89	2.48	0.04	0.003
17.78	18.20	1.66	−0.10	2.29	0.04	0.003

4. Discussion

The present mapping and astrometry of SiO $v = 1$ $J = 5 \rightarrow 4$ masers in W 43A pinpoint the driving source of the bipolar fast jet at the brightness peak of the 1.3 mm continuum source within ∼20 au. In order to localize the jet's driving source more accurately, one may need to find the three-dimensional kinematics of the masers through measurement of their relative proper motions as made for SiO $v = 1$ $J = 1 \rightarrow 0$ masers in Orion Source I (L. D. Matthews et al. 2010).

The differences in the SiO maser distributions among different rotational transitions have been modeled theoretically, suggesting maser excitation in different physical conditions within the same CSE (e.g., M. D. Gray et al. 2009). Note, however, that the model calculations have been limited to lower rotational transitions (up to $J = 4 \rightarrow 3$). It has been observationally found that SiO $v = 1$ $J = 1 \rightarrow 0$ masers in evolved stars tend to be excited closer to the central star than higher-transition SiO maser lines (e.g., D.-H. Yoon et al. 2018). While this is seen in SiO masers with a ring-shaped distribution, we also see this trend in the masers presented in

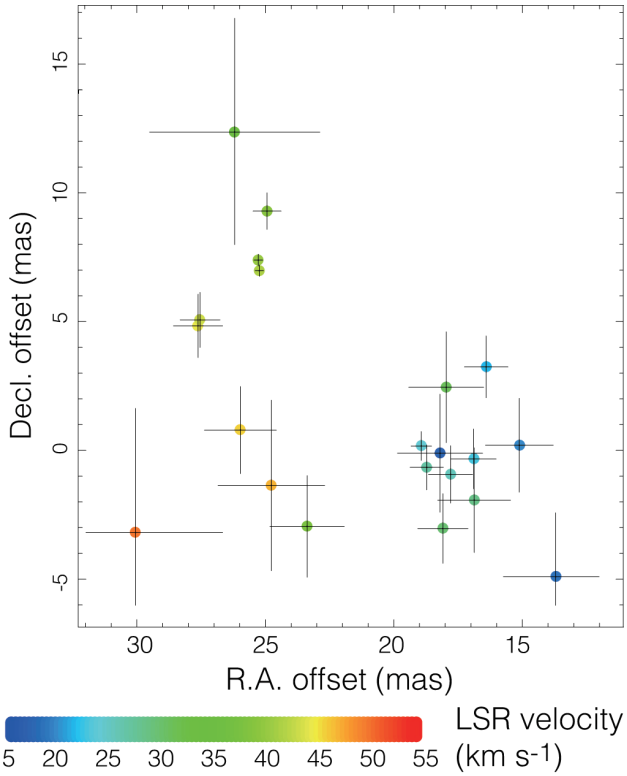

Figure 3. Distribution of SiO $v = 1$ $J = 1 \rightarrow 0$ maser spots observed in W 43A with the VLA on 2004 December 7. The map origin is at the phase-tracking center of the observation at (R.A., decl.) (J2000.0) = $18^{\rm h}47^{\rm m}41\overset{\rm s}{.}1618$, $-01°45'11\overset{''}{.}538$).

this paper, which trace a bipolar outflow, with SiO $v = 1$ $J = 5 \rightarrow 4$ maser emission tracing a larger structure than the $J = 1 \rightarrow 0$.

Significant changes in the distributions of the SiO $J = 5 \rightarrow 4$ and $J = 1 \rightarrow 0$ masers are unlikely expected within the time gap between the ALMA and VLA observations ($\sim$15 yr) and the possible duration of maser excitation ($\lesssim$100 yr) even throughout the evolution of the jet and outflow. In fact, the LoS velocity coverage of the SiO $v = 1$ $J = 1 \rightarrow 0$ masers in W 43A had remained unchanged while they had been observed for several years (J.-I. Nakashima & S. Deguchi 2003; H. Imai et al. 2005). As presented in Section 3.3, the distribution of the SiO $v = 1$ $J = 1 \rightarrow 0$ masers had been stable in $\sim$1.5 yr, although the lifetimes of the individual maser features look shorter than that interval. It also has been found that SiO maser sources that exhibit a bipolar spatiokinematic structure are always associated with the very vicinity of the driving source of the bipolar outflows, although the number of such bipolar SiO maser sources is limited (Orion Source I—L. D. Matthews et al. 2010; S. Issaoun et al. 2017; W51 IRS 2—J. A. Eisner et al. 2002). Note that the travel time of the outflow in the SiO maser region is already comparable to or shorter than the timescales mentioned above. Therefore, these SiO masers would have been always excited and quenched in the limited area close to the driving source of the outflow. In conclusion, the significant difference in the distributions of SiO $J = 5 \rightarrow 4$ and $J = 1 \rightarrow 0$ masers presented in this paper may be intrinsic through the duration of the maser excitation.

The similarity in the velocity ranges of these masers suggests that the $J = 5 \rightarrow 4$ masers may be also associated with a biconical flow of the entrained material, as seen in the $J = 1 \rightarrow 0$ masers, along a large opening angle around the collimated jet. On the other hand, the significant difference in the LoS velocity gradient and the distribution extent seen in the SiO $v = 1$ $J = 5 \rightarrow 4$ and 1612 MHz OH masers from those of the SiO $v = 1$ $J = 1 \rightarrow 0$ and H_2O masers can be explained by different velocity gradients and maser amplification gains between the blue- and redshifted sides of the maser regions, as well as different opening angles of the inner and outer parts of the outflow.

Figure 4 sketches out a toy model of the jet and outflow in W 43A. H. Imai et al. (2002) have already suggested the existence of a highly collimated, high-velocity bipolar jet and a spherically and slowly expanding CSE. Paper I added the suggestion of the existence of a moderately collimated intermediate-velocity outflow composed of material entrained and accelerated outward by the jet. Our model proposes that both the SiO $v = 1$ $J = 5 \rightarrow 4$ and $J = 1 \rightarrow 0$ masers are associated with this entrained outflow.

In order to explain the similar ranges but the opposite gradients of the maser LoS velocities between the $J = 5 \rightarrow 4$ and $J = 1 \rightarrow 0$ masers, we suppose that they are associated with different stream lines of the outflow at different opening angles from the driving point of the jet with respect to the major axis of the jet. Taking into account the relatively large velocity dispersion of the blue- and redshifted lobes of the $J = 1 \rightarrow 0$ masers, as shown in Figure 3, one can suppose that they are associated with a slowly expanding (and rotating) outflow, as shown in the SiO masers in Orion Source I (L. D. Matthews et al. 2010), covering a wider range of the opening angle of the outflow. On the other hand, the outer region of the the outflow hosting the $J = 5 \rightarrow 4$ masers may be

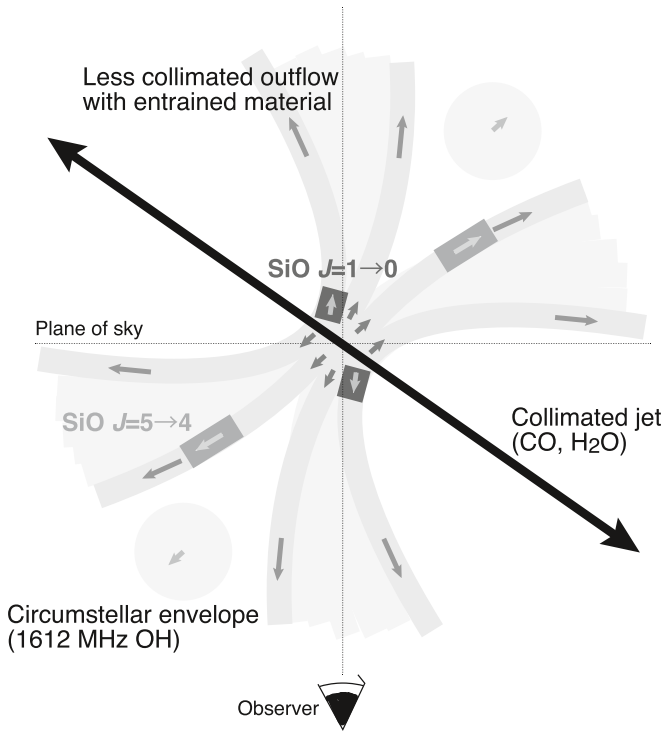

Figure 4. Sketch of a model that is composed of a highly collimated, bipolar jet, a less collimated, moderate-velocity outflow around the jet, and an outer, slowly expanding CSE in W 43A, which may host H_2O SiO (both of the $J = 5 \rightarrow 4$ and $J = 1 \rightarrow 0$ transitions), and 1612 MHz OH masers, respectively.

further accelerated, causing a larger velocity gradient along the stream lines, making velocity-coherent regions along the LoS for maser amplification in the stream lines closer to the jet's axis. This makes the LoS velocity coverage of the $J = 5 \rightarrow 4$ masers closer to that of the $J = 1 \rightarrow 0$ masers. The velocity-coherent regions may be formed at only one of the sides in each jet lobe, either in the background or the foreground from the jet axis. Such velocity-coherent regions for SiO maser amplification are modeled in more detail by H. Imai et al. (2005).

The hypothesis of the driving source and the spatiokinematical structure of the jet and outflow described above will be diagnosed through comparison with the data of CO $J = 2 \rightarrow 1$ emission in a separate paper. These works are crucial to explore the possible host star supplying its mass-loss material to its companion driving the jet.

The central, independent, 1.3 mm continuum peak emission of dust looks spatially unresolved with ALMA's synthesized beam (Figure 1), implying an upper limit of the dust CSE size to $\sim$80 au. It is difficult to interpret the source as just a segment of the material swept by the jet rather than the main body of the CSE of the host star mentioned above. Here suppose a CEE system, as suggested (T. Khouri et al. 2021) within the coincident scale mentioned above. This is supported by clear symmetry of the distributions of SiO maser emission over that scale. The mass of each star is suggested to be $M_* < 4\,M_\odot$ on the basis of the isotopic ratios of oxygen in the CSEs/jets of WFs (T. Khouri et al. 2021). The orbital period of this binary system is implied to be $P_{\rm orb} = 5$–7 yr on the basis of the time spacing of periodic and heavy mass ejection indicated in the W 43A jet (Paper I). These two values give an upper limit of the orbital radius to $\sim$6 au for W 43A. This

upper limit is consistent with the orbital radius necessary to create a common envelope, since the corresponding upper limit to the Roche lobe of the binary ($\lesssim$3 au) is close to the typical radii of AGB stars (1–2 au). Note that W 43A may host an OH/IR star with a pulsation period of ∼400 days (J. Herman & H. J. Habing 1985), supporting the typical radius value. ALMA's higher angular resolution (up to 10 mas) may spatially resolve the continuum emission and pinpoint the host star with respect to the SiO masers at possibly higher rotational transitions.

The size of the central stellar system or the orbit parameters of the possible binary system should be derived by such observations more directly and accurately for providing the strong constraint on the driving mechanism of a jet and its entrained outflow with an extremely short lifetime ($\lesssim$200 yr) and an extremely high mass-loss rate ($\gtrsim 10^{-3}\,M_{\odot}\,\mathrm{yr}^{-1}$; T. Khouri et al. 2021). Adding the information of the whole CSE structure that should be mapped in more detail (see B. H. K. Yung et al. 2017), it will be elucidated how to supply massive jet/outflow material in a possible CEE system to the central stellar system through the region of the SiO maser excitation.

Acknowledgments

This paper makes use of the ALMA data, ADS/JAO. ALMA# 2016.1.00540.S and 2018.1.00190.S. ALMA is a partnership of ESO (representing its member states), NSF (USA), and NINS (Japan), together with NRC (Canada), MOST and ASIAA (Taiwan), and KASI (Republic of Korea), in cooperation with the Republic of Chile. The Joint ALMA Observatory is operated by ESO, AUI/NRAO, and NAOJ. The VLA is operated by the National Radio Astronomy Observatory (NRAO) under cooperative agreement by Associated Universities, Inc. H.I. was supported by the MEXT/JSPS KAKENHI program (16H02167). J.F.G. is supported by grants PID2020-114461GB-I00, PID2023-146295NB-I00, and CEX2021-001131-S, funded by MCIN/AEI/10.13039/501100011033. H.I. and J.F.G. were supported by the Invitation Program for Foreign Researchers of the Japan Society for Promotion of Science (JSPS grant S14128).

Facilities: ALMA, VLA (NRAO).

Software: AIPS, CASA.

Appendix
List of Molecular Lines Detected in the ALMA Data

Table 3 lists the molecular lines detected in the ALMA data taken on 2019 July 13 in the code 2018.1.00190.S. Except SiO $v = 1\ J = 5 \rightarrow 4$ presented in this paper, they will appear in our future publications (T. Hoshino et al. 2025, in preparation). Note that the largest angular scale recovered in the observation for extended thermal emission is around 500 mas.

Table 3
Molecular Lines Detected in the ALMA Data toward W 43A

Molecule	Transition	Rest Frequency (MHz)	LSR Velocity (km s^{-1})
SiO	$v = 1\ J = 5 \rightarrow 4$	215,596.068	See Table 1
$CH_3CH_2^{13}CN$?	$J_{Ka,Kc} = 14_{3,11} \rightarrow 14_{1,13}$?	215,453.841?	215,466–215,493 MHz
p-H_2S	$J_{Ka,Kc} = 14_{2,0} \rightarrow 2_{1,1}$	216,710.437	−60–135
SiO	$v = 0\ J = 5 \rightarrow 4$	217,104.984	−72–142
$C^{18}O$	$v = 0\ J = 2 \rightarrow 1$	219,560.358	∼37
SO	$(N, J) = (5, 6) \rightarrow (4, 5)$	219,949.433	−66–130
^{13}CO	$v = 0\ J = 2 \rightarrow 1$	220,398.684	−60–128
OCS	$J = 19 \rightarrow 18)$	231,060.993	5–70
CO	$v = 0\ J = 2 \rightarrow 1$	230,538.000	−69–139

ORCID iDs

Hiroshi Imai https://orcid.org/0000-0002-0880-0091
Daniel Tafoya https://orcid.org/0000-0002-2149-2660
José F. Gómez https://orcid.org/0000-0002-7065-542X
Jun-ichi Nakashima https://orcid.org/0000-0003-3324-9462
Gabor Orosz https://orcid.org/0000-0002-5526-990X

References

Chong, S.-N., Imai, H., & Diamond, P. J. 2015, ApJ, 805, 53
Eisner, J. A., Greenhill, L. J., Herrnstein, J. R., Moran, J. M., & Menten, K. M. 2002, ApJ, 569, 334
Gómez, J. F., Suárez, O., Rizzo, J. R., et al. 2017, MNRAS, 468, 2081
Gray, M. 2012, Maser Sources in Astrophysics (Cambridge: Cambridge Univ. Press)
Gray, M. D., Wittkowski, M., Scholz, M., et al. 2009, MNRAS, 394, 51
Herman, J., & Habing, H. J. 1985, A&AS, 59, 523
Imai, H., Hamae, Y., Amada, K., et al. 2023, PASJ, 75, 1183
Imai, H., Nakashima, J.-i., Diamond, P. J., Miyazaki, A., & Deguchi, S. 2005, ApJL, 622, L125
Imai, H., Obara, K., Diamond, P. J., Omodaka, T., & Sasao, T. 2002, Natur, 417, 829
Imai, H., Sahai, R., & Morris, M. 2007, ApJ, 669, 424
Imai, H., Uno, Y., Maeyama, D., et al. 2020, PASJ, 72, 58
Issaoun, S., Goddi, C., Matthews, L. D., et al. 2017, A&A, 606, A126
Khouri, T., Vlemmings, W. H. T., Tafoya, D., et al. 2021, NatAs, 6, 275
Matthews, L. D., Greenhill, L. J., Goddi, C., et al. 2010, ApJ, 708, 80
Nakashima, J.-I., & Deguchi, S. 2003, PASJ, 55, 229
Orosz, G., Gómez, J. F., Imai, H., et al. 2019, MNRAS, 482, L40
Reid, M. J., Dame, T. M., Menten, K. M., & Brunthaler, A. 2016, ApJ, 823, 77
Sakai, N., Nakanishi, H., Kurahara, K., et al. 2022, PASJ, 74, 209
Tafoya, D., Franco-Hernández, R., Vlemmings, W. H. T., Pérez-Sánchez, A. F., & Garay, G. 2014, A&A, 562, L9
Tafoya, D., Imai, H., Gómez, J. F., et al. 2020, ApJL, 890, L14
Vlemmings, W. H. T., Diamond, P. J., & Imai, H. 2006, Natur, 440, 58
Yoon, D.-H., Cho, S.-H., Yun, Y., et al. 2018, NatCo, 9, 2534
Yung, B. H. K., Nakashima, J.-i., Hsia, C.-H., & Imai, H. 2017, MNRAS, 465, 4482